DOI: 10.1002/ejic.200601181

Structural, Electrochemical, and Spectroscopic Properties of a Class of Dodecasubstituted Iron Porphyrins Bearing Four Positive Charges Close to the Metal

Mark W. Renner,[a] Constance Bochot,[b] Annie Héroux,[c] Daniel Mansuy,[b] and Pierrette Battioni*[b]

Keywords: Iron / Porphyrins / Ligand design / X-ray diffraction / Voltammetry

The first iron complexes of the tetracationic 2,3,7,8,12,13,17,18-octaethyl-5,10,15,20-tetra-*N*-pyridiniumylporphyrin, (OEPy$_4$P)$^{4+}$, in which four pyridine molecules are attached to the *meso*-carbon atoms through their nitrogen atoms, were synthesized in three steps starting from Zn(OEP) (Zn-β-octaethylporphyrin) with an overall yield of ca. 30 %. The X-ray structure of [Fe^{II}(OEPy$_4$P)(pyridine)$_2$](CF$_3$SO$_3$)$_3$(Br) established that the molecule adopts a severely distorted nonplanar saddle conformation. ^{1}H NMR spectroscopy showed that the [Fe^{II}(OEPy$_4$P)(B)$_2$]$^{4+}$ ligated complexes, B = pyridine (Py) or imidazole (Im), are low-spin, Fe^{II}, S = 0. These complexes exhibit redox potentials for the Fe^{III}/Fe^{II} couple that range between 0.62 and 0.38 V (vs. Ag/AgCl) and are shifted by as much as +0.7 V relative to those of the corresponding planar iron complexes of OEP and of the nonplanar complexes of OETPP. Such highly positive redox potentials explain the stability of these iron(II) porphyrins in air. As previously found for dodecasubstituted iron porphyrins bearing electron-withdrawing groups, the UV/Vis spectra of the [Fe^{II}(OEPy$_4$P)(B)$_2$]$^{4+}$ complexes exhibit Soret and visible bands which are redshifted by ca. 40 nm relative to those of Fe(OEP)(Py)$_2$. These metallo-OEPy$_4$P^{4+}complexes offer promising synthetic avenues to novel classes of highly charged porphyrins and multiporphyrin arrays, which are soluble in aqueous and polar organic solvents.

Introduction

Many porphyrin cofactors that are present in living systems, such as photosynthetic reaction centers, light harvesting antenna complexes, and heme proteins, exhibit nonplanar macrocycles.[1] Such macrocycle distortions are believed to influence the biological functions of these cofactors. In vivo, the scaffolding, hydrogen bonding, macrocycle saturation, and axial ligation modulate the porphyrin conformations. In model porphyrins, specific macrocycle configurations have been generated by introduction of bulky and multiple peripheral substituents. By varying the macrocycle modes and degrees of distortion, as well as the nature of the metal, the chemical and physical properties of the tetrapyrroles can thus be fine-tuned. Indeed, such nonplanar distortions have been shown to alter the redox, magnetic, electronic, ligand binding, and excited-state properties of metalloporphyrins.[1,2]

In some cytochromes, the heme iron is coordinated by two axial histidine residues whose relative orientation with respect to each other can alter both their spectroscopic and redox properties.[1,3] In model studies of bis-ligated iron porphyrins, the relative and absolute orientation of the axial ligands have also been shown to modulate the electronic structure, and the magnetic and redox properties of the hemes.[3] In the numerous crystal structures of bis-ligated iron porphyrins reported so far, the relative orientations of the axial ligands are preferentially perpendicular in Fe^{III} and parallel in Fe^{II} porphyrins.[3,4] However, structures of iron(II) porphyrins with perpendicular axial pyridine or imidazole orientations have been reported in which this orientation was controlled by steric interactions imposed by the porphyrin and its substituents.[3,4] As well, crystallographic studies of highly saddled metalloporphyrins have further shown that the combination of macrocycle distortion and peripheral substituents forms trenches which tend to orient the axial ligands perpendicular to each other.[5]

Many dodecasubstituted porphyrins have been synthesized, most of which exhibit nonplanar, highly distorted structures.[1,2] Iron and manganese porphyrins bearing up to twelve electron-withdrawing substituents are especially interesting because of their significantly altered redox potentials and their catalytic properties.[1,6–9] Dodecasubstituted metalloporphyrins bearing multiple charges should be

[a] Condensed Matter Physics and Materials Science Department, Brookhaven National Laboratory,
Building 555, Upton, NY 11973-5000, USA
[b] UMR 8601, Laboratoire de Chimie et Biochimie Pharmacologiques et Toxicologiques, Université Paris 5
45 rue des Saints-Pères, 75270 Paris Cedex 06, France
[c] Biology Department, Brookhaven National Laboratory
Upton, NY 11973-5000, USA

Supporting information for this article is available on the WWW under http://www.eurjic.org or from the author.

of particular interest because of their solubility in water and their possible interactions with various biological targets such as proteins and nucleic acids. Water-soluble metalloporphyrins exhibit interesting properties as photosensitizers for photodynamic therapy of cancer,[10] and as antimalarial,[11] antibacterial,[12] anti-HIV,[13,14] and antiprion[15] agents. Moreover, cationic metalloporphyrins have been explored for the treatment of pathologies in which the superoxide radical and its progeny are suspected of playing important roles.[16–19] *N*-methylpyridiniumyl-*meso*-substituted metalloporphyrins have been used very often for this purpose. This is indeed the case for the first reported dodecasubstituted tetracationic metalloporphyrins that were derived from β-octabromo-*meso*-tetra(*N*-methylpyridiniumyl)porphyrin.[16]

Recently, a polycationic porphyrin bearing 20 positive charges was obtained by nucleophilic substitution of the F substituents of *meso*-tetra(pentafluorophenyl)porphyrin (H_2TFPP) with 4-dimethylaminopyridine in the presence of trimethysilyl triflate.[20] Moreover, a tetracationic Zn^{II} dodecasubstituted porphyrin, $Zn(OEPy_4P)^{4+}$ ($OEPy_4P$: β-octaethyl-*meso*-tetra-(pyridiniumyl-1)porphyrinato) (Scheme 1), bearing four pyridinium groups bound at the *meso* position through their nitrogen atom, was reported.[21] It was the first representative of a new class of dodecasubstituted, nonplanar metalloporphyrins bearing four positive charges less than 5 Å from the metal center. Even more recently, the corresponding free-base porphyrin $H_2OEPy_4P^{4+}$, and its Mn complexes, were synthesized.[22] The latter are new biomimetic hydroxylation catalysts that exhibit good solubility in both polar aprotic solvents and water.[22]

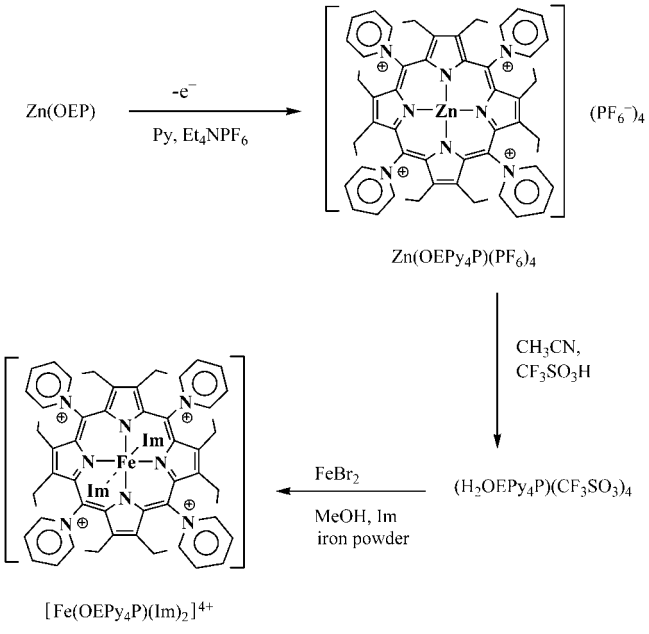

Scheme 1. Synthesis of $[Fe(OEPy_4P)(Im)_2]^{4+}$ in three steps from Zn(OEP).

We report here the synthesis and the spectral and electrochemical properties of iron complexes of $H_2OEPy_4P^{4+}$, and the first X-ray structure of a bis(pyridine)Fe^{II} complex of this novel class of tetracationic dodecasubstituted porphyrins. These metallo-$OEPy_4P^{4+}$ complexes offer promising synthetic avenues to additional novel classes of highly charged porphyrins and multiporphyrin arrays that are soluble in aqueous and polar organic solvents.[23]

Results and Discussion

Synthesis of $[Fe(OEPy_4P)(Im)_2]^{4+}$

The iron complex of $OEPy_4P$ was prepared in three steps starting from Zn(OEP) (OEP: β-octaethylporphyrinato) (Scheme 1). The first step that led to $[Zn(OEPy_4P)](PF_6)_4$ was done according to published procedures[21] (Scheme 1). Demetallation of this Zn complex involved its treatment with excess CF_3SO_3H,[24,25] which led to the $CF_3SO_3^-$ salt of $[H_2OEPy_4P]^{4+}$ in a 80% yield.[22] The last step, the insertion of iron, was done under an atmosphere of argon by using 2.5 equiv. of $FeBr_2$ in the presence of imidazole (Im) and iron powder. The resulting complex was found to be a diamagnetic Fe^{II} complex of $OEPy_4P$ including two axial imidazole ligands as shown by ^{1}H NMR spectroscopy. Its ^{1}H NMR spectrum exhibits all the signals expected for the pyridinium (in the 8.5–10.5 ppm region) and ethyl (in the 0.5–2.6 ppm region) substituents of the porphyrin ring, and for the imidazole ligands (signals at δ = 3.05, 3.83, and 5.20 ppm) (see Experimental Section). Integration of these signals is consistent with two imidazole ligands per porphyrin. In the presence of excess imidazole, the signals of the free and bound imidazole coexist in the ^{1}H NMR spectra, which indicates that the exchange between free and bound imidazole is slow on the NMR time scale. Temperature-dependent ^{1}H NMR spectroscopic studies performed in CD_3OD in the presence of either 5 or 50 equiv. of imidazole, between 300 and 200 K, did not show significant changes in the shape of the peaks, and only showed small variations in the chemical shifts.

A high resolution mass spectrometry (HRMS) analysis of the $[Fe(OEPy_4P)(Im)_2]^{4+}$ complex, with the use of nanoelectrospray ionization and Fourier transform mass spectrometry (nano-ESI-FTMS), showed a molecular ion at m/z = 1496.2405, which corresponds to $[Fe(OEPy_4P)(CF_3SO_3)_4]^+$ (monoisotopic m/z calculated for $C_{60}H_{60}N_8S_4O_{12}F_{12}Fe$ = 1496.2368; isotopic distribution of the peaks cluster identical to that calculated for the above formula). This molecular ion should derive from the $[Fe(OEPy_4P)(Im)_2](CF_3SO_3)_4$ complex having lost its two axial ligands under the MS conditions, as usually found for such Fe(porphyrin)$(Im)_2$ complexes. A smaller peak at m/z = 1426.1999, which corresponds to $[Fe(OEPy_4P)(CF_3SO_3)_3(Br)]^+$ (theoretical monoisotopic m/z = 1426.2033; isotopic distribution in agreement with the formula $C_{59}H_{60}N_8S_3O_9F_9BrFe$), was also observed. This peak should come from the $[Fe(OEPy_4P)(Im)_2](CF_3SO_3)_3(Br)$ complex, which was present in the analyzed sample as a result of the exchange of a $CF_3SO_3^-$ counterion of $[Fe(OEPy_4P)(Im)_2](CF_3SO_3)_4$ by Br^- coming from $FeBr_2$ in the metallation step. The presence of such a $[Fe(OEPy_4P)(Im)_2]^{4+}$

complex associated with three $CF_3SO_3^-$ counterions and one Br^- counterion is in agreement with the X-ray study performed on the complex obtained by replacement of the Im ligands with pyridine. This X-ray study definitely established a $[Fe(OEPy_4P)(Py)_2](CF_3SO_3)_3(Br)$ structure for the latter complex (see below). Obviously, the nature of the counterions of these $[Fe(OEPy_4P)(B)_2]^{4+}$ complexes, with B = Im or Py, should greatly depend on the synthesis protocol and on the medium in which they are studied. Therefore, these complexes will simply be called $[Fe(OEPy_4P)(B)_2]^{4+}$ in the following sections.

The UV/Vis spectra of $[Fe(OEPy_4P)(B)_2]^{4+}$, with B = Im or Py, exhibit Soret and visible bands that are all redshifted ca. 40 nm relative to $Fe^{II}(OEP)(Py)_2$ (Table 1). These UV/Vis spectra are similar to those of the previously reported low-spin bispyridine dodecasubstituted Fe^{II} porphyrins bearing electron-withdrawing groups [see $Fe(F_{20}DPP)(Py)_2$ in Table 1, $F_{20}DPP$: β-octaphenyl-*meso*-tetrapentafluorophenylporphyrinato], whereas they clearly differ from the spectra of $[Fe^{III}(porphyrin)(Py)_2]^+$ and $Fe^{II}(porphyrin)$ complexes (Table 1). The redshifted optical spectra of $[Fe(OEPy_4P)(B)_2]^{4+}$ are likely due to the presence of the four electron-withdrawing pyridinium substituents and to the distorted structure of the porphyrin macrocycle (see below), relative to that of $Fe^{II}(OEP)(Py)_2$ which is planar.[4] In distorted porphyrins, the highest occupied molecular orbital (HOMO) is destabilized more than the lowest unoccupied orbital (LUMO), which results in a decrease in the HOMO to LUMO energy gap and a redshift in the absorption bands.[26–28]

Table 1. UV/Vis characteristics of the $[Fe(OEPy_4P)(B)_2]^{4+}$ complexes and related iron porphyrins.[a]

Compound	Solvent	λ_{max} [nm, Soret]
$Fe(F_{20}DPP)$[37]	benzonitrile	327, 432, 534, 586
$Fe(F_{20}DPP)(Py)_2$[37]	pyridine	351, 447, 551, 588
$[Fe(Br_8TFPP)(Py)_2]^+$[33]	CH_2Cl_2	454, 556, 588
$[Fe(OEP)(Py)_2]Cl$[38]	pyridine	396, 510, 529, 625
Fe(OEP)[39]	CH_2Cl_2	405, 531, 556
$Fe(OEP)(Py)_2$[40]	pyridine	408, 517, 546
$[Fe(OEPy_4P)(Py)_2]^{4+}$[a]	MeCN, Py	366, 439, 458, 556, 588
$[Fe(OEPy_4P)(Im)_2]^{4+}$[a]	MeCN, Im	366, 458, 568, 601

[a] This work, spectra in MeCN containing 5% Py or 100 μM Im.

Electrochemical Properties of $[Fe(OEPy_4P)(B)_2]^{4+}$

The redox chemistry of these iron complexes was studied by cyclic voltammetry (Figure 1 and Table 2). The $E_{1/2}$ values for $[Fe(OEPy_4P)(Im)_2]^{4+}$ and $[Fe(OEPy_4P)(Py)_2]^{4+}$ are +0.38 and +0.62 V respectively, vs. Ag/AgCl in MeCN. The $E_{1/2}$ peak potential separations for these complexes are 100 and 60 mV, respectively. The $Fe^{III/II}$ couple is obviously sensitive to the axial ligands and shifts − 240 mV upon replacement of the pyridine groups with imidazole moieties. For bis-ligated Fe^{III} porphyrins, the $Fe^{III/II}$ $E_{1/2}$ potential undergoes a negative shift as the pKa of the axial ligands increases.[6] The electron-withdrawing *meso*-pyridinium substituents on the porphyrin shift the $Fe^{III/II}$ couple anodically, which stabilizes the iron(II) oxidation state. The redox potentials of iron porphyrins with a varying number of electron-withdrawing substituents have been reported, and the $Fe^{III/II}$ redox couple undergoes a positive shift with an increasing number of electron-withdrawing groups.[6,29] Comparison of the $E_{1/2}$ of $Fe(OETPP)(B)_2$ (OETPP: β-octaethyl-*meso*-tetraphenylporphyrinato) and $[Fe(OEPy_4P)(B)_2]^{4+}$ shows a large positive shift in the metal redox potentials upon replacing the *meso*-phenyl with *meso*-pyridinium groups (+730 mV and +870 mV for B = Im and Py, respectively, Table 2). Because these compounds have similar nonplanar conformations (see below), electronic, rather than structural, factors seem to cause this large positive shift.

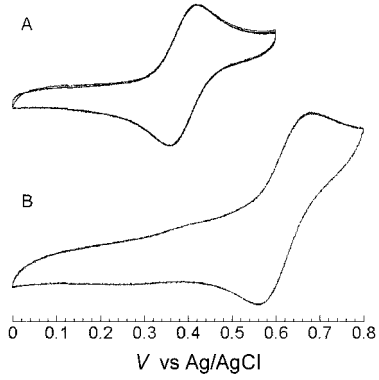

Figure 1. Cyclic voltammograms of $[Fe(OEPy_4P)(Im)_2]^{4+}$ (A) and $[Fe(OEPy_4P)(Py)_2]^{4+}$ (B) in MeCN containing 0.1 M TBAP. Scan rate: 100 mV s^{-1}.

Table 2. Electrochemical data for the $[Fe(OEPy_4P)(B)_2]^{4+}$ complexes and related iron porphyrins.

Compound	Fe^{III}/Fe^{II} [V]	Conditions[a]
$[Fe(OEP)(Py)_2]^+$[41]	–0.02	PrCN, TBAP, SCE
$[Fe(OEP)(1\text{-}MeIm)_2]^+$[41]	–0.39	CH_2Cl_2, TBAP, SCE
$[Fe(F_{20}DPP)(Py)_2]^+$[41]	+0.53	Pyr, TBAP, SCE
$[Fe(Br_8TFPP)(Py)_2]^+$[33]	+0.82	CH_2Cl_2, TBAP, Ag/AgCl
$[Fe(OETPP)(Im)_2]^+$[b]	–0.31	PrCN, TBAP, SCE
$[Fe(OETPP)(Py)_2]^+$[b]	–0.21	PrCN, TBAP, SCE
$[Fe(OEPy_4P)(Py)_2]^{4+}$[c]	+0.62	MeCN, TBAP, Ag/AgCl
$[Fe(OEPy_4P)(Im)_2]^{4+}$[c]	+0.38	MeCN, TBAP, Ag/AgCl

[a] Redox potentials were measured in the indicated solvent containing 0.1 M TBAP (tetrabutylammonium perchlorate). Values are in V relative either to the saturated calomel electrode (SCE) or to the Ag/AgCl electrode. [b] M. W. Renner and J. Fajer, unpublished results. [c] This work.

Two electronic structures are theoretically possible for $S = 0$ $Fe(porphyrin)(L)_2$ complexes, a low-spin d6 Fe^{II} porphyrin structure and a structure involving a low-spin d5 Fe^{III} ion antiferromagnetically coupled to a porphyrin radical. However, presently, there is no indication in favor of the latter structure for all the $S = 0$ $Fe(porphyrin)(L)_2$ complexes published so far in the literature. An electronic structure resulting from an intramolecular electron transfer from Fe^{II} to the porphyrin should be favored by the presence of porphyrin electron withdrawing substituents. However,

Mössbauer data of the β-octanitrated Fe[TDCP$(NO_2)_8$P]-$(EtOH)_2$ complex, which exhibits the highest redox potential described so far for a Fe(porphyrin)$(L)_2$ complex (1030 mV vs. SCE[30]), clearly showed that it is a Fe^{II} complex.[30] Moreover, metal(porphyrin radical) complexes usually exhibit a characteristic porphyrin radical absorption in the 700–1000 nm region; for instance Zn^{II}[TDCP$(NO_2)_7$-P]$^{\cdot-}$ and Ni^{II}[TDCP$(NO_2)_7$P]$^{\cdot-}$ complexes show bands at 900 and 770 nm, respectively.[31] However, the UV/Vis spectra of [Fe$(OEPy_4P)(Im)_2]^{4+}$ and [Fe$(OEPy_4P)(Py)_2]^{4+}$ failed to show any band in the 700–1000 nm region. Finally, the ^{1}H NMR spectra of [Fe$(OEPy_4P)(B)_2]^{4+}$ complexes exhibit peaks, whose shapes and chemical shifts are highly similar to those of Zn[$(OEPy_4P)]^{4+}$ and H_2[$(OEPy_4P)]^{4+}$ in which the porphyrin ligand does not involve any radical species. All these data are in favor of the low-spin d6 Fe^{II} porphyrin electronic structure, as the one proposed for all the previously described $S = 0$ Fe(porphyrin)$(L)_2$ complexes.[4]

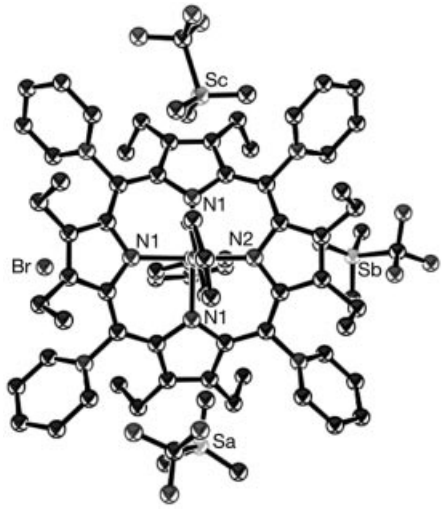

Figure 2. ORTEP diagram of **1** with the anions included. The thermal ellipsoids are drawn at the 30% probability level.

Structural Studies

Owing to the small crystal size ($0.6 \times 0.4 \times 0.1$ mm) and quality, the X-ray diffraction experiments were performed with the use of high intensity X-rays from the National Synchrotron Light Source at Brookhaven National Laboratory beamline X26C. The molecular structure of [Fe(OE-$Py_4P)(Py)_2](CF_3SO_3)_3(Br)$ (**1**) and the atom numbering scheme are displayed in Figures 2 and 3. Selected bond lengths and angles are listed in Table 3. [Fe$(OEPy_4P)$-$(Py)_2]^{4+}$ crystallizes with four anions, three $CF_3SO_3^-$, and one Br^-, which are located between adjacent *meso*-pyridinium groups and above the pyrrole rings (Figure 2). One of the original $CF_3SO_3^-$ ions of the free base must therefore have been replaced by a Br^- during the metal insertion reaction with $FeBr_2$. The molecular structure of **1** exhibits a S_4 saddle-shape distortion with an absolute displacement of 1.22 Å for the pyrrole C_β atoms relative to the 24-atom plane; an edge-on view of **1** is shown in Figure 3. The displacements of the porphyrin atoms from the 24-atom core, the axial ligand plane orientations, and a "clothesline" representation of the macrocycle distortions are shown in Figure 4.

The trenches formed by the nonplanar porphyrin conformation and the β-ethyl groups align the axial pyridines perpendicular to each other and along the N_p–Fe–N_p axes. The dihedral angle between the axial pyridine and the closest N_p–Fe–N_{ax} plane (ϕ) are 11.2 and 13.3° for pyridine N9 and N10, respectively. The pyridines are effectively orthogonal to each other with a dihedral angle between the two axial pyridine planes of 87°. A comparison of the structural parameters of **1** and other related bispyridine iron porphyrins are listed in Table 4. As with other bispyridine iron(II) porphyrins,[4] the iron atom resides in the $4N_p$ plane, displaced 0.01 Å toward the axial pyridine N10. The axial pyridines are approximately perpendicular to the macrocycle plane with dihedral angles of 81.1° and 89.3° for pyridine N9 and N10, respectively. Pyridine N9 is tilted ca. 9° relative to the $4N_p$ plane which could be a result of hydrogen bonding between the pyridine C–H and the oxygen atom of a nearby $CF_3SO_3^-$ anion; the C59···O distance is 3.33 Å.

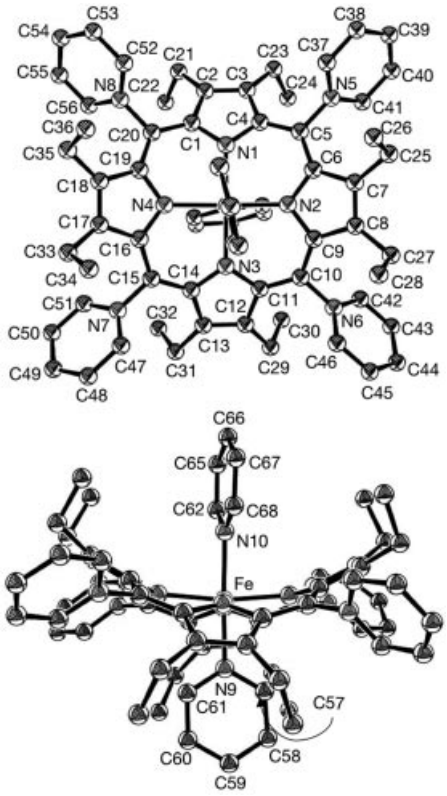

Figure 3. Molecular structure and numbering scheme for **1**, thermal ellipsoids drawn at the 30% probability level; the hydrogen atoms and the counterions are removed for clarity.

Typically, for bis-ligated low-spin iron(II) porphyrins[4] the equatorial Fe–N_p distances are ca. 2.00 Å. The average equatorial Fe–N_p distance in complex **1** [1.953(3) Å] is slightly shorter than in the dodecasubstituted complexes [Fe^{III}(OETPP)$(Py)_2]ClO_4$ at 80 K [1.957(3) Å] and Fe^{II}-

Table 3. Selected bond lengths and bond angles for [Fe^{II}(OE-Py_4P)$(Py)_2$]$(CF_3SO_3)_3$(Br) (**1**).

Bond	Distance [Å]	Bond	Distance [Å]
Fe–N1	1.955(3)	Fe–N4	1.958(3)
Fe–N2	1.949(3)	Fe–N5	2.028(3)
Fe–N3	1.951(3)	Fe–N6	2.027(3)
N1–C1	1.382(4)	N2–C6	1.380(4)
N1–C4	1.372(4)	N2–C9	1.375(4)
C1–C2	1.453(5)	C6–C7	1.455(5)
C2–C3	1.366(5)	C7–C8	1.359(5)
C3–C4	1.459(5)	C8–C9	1.457(5)
C4–C5	1.392(5)	C9–C10	1.389(5)
C5–C6	1.390(5)	C10–C11	1.393(5)
C5–N5	1.463(5)	C20–N8	1.463(4)
Angle	Value [°]	Angle	Value [°]
N1–Fe–N2	89.79(12)	N1–C4–C5	119.1(3)
N2–Fe–N3	91.46(12)	N1–C1–C20	118.7(3)
N3–Fe–N4	90.29(12)	C1–N1–C4	105.2(3)
N1–Fe–N4	89.99(12)	C2–N1–C20	130.6(3)
N1–Fe–N3	169.98(13)	C1–C2–C3	106.4(3)
N2–Fe–N4	171.11(13)	C2–C3–C4	106.3(3)
N1–Fe–N9	85.99(12)	C3–C4–C5	130.3(3)
N1–Fe–N10	97.20(12)	C4–C5–C6	126.6(3)
N1–C1–C2	110.4(3)	C4–C5–N6	115.9(3)
N1–C4–C3	110.6(3)	C1–C20–N8	115.7(3)

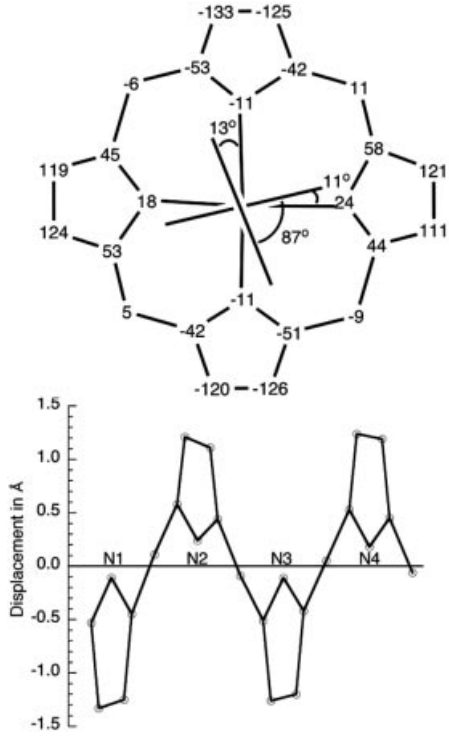

Figure 4. Top: Displacements of the 24-atom core in units of 0.01 Å and the orientation of the axial pyridine ligand planes of **1**. Bottom: Linear display of the out-of-plane displacements of the core atoms of **1** from the average plane of the 24 atoms (the horizontal axis is not to scale).

$(Br_8TFPP)(Py)_2$ (Br_8TFPP: β-octabromo-*meso*-tetrapentafluorophenylporphyrinato) [1.963(7) Å].[32,33] The increased distortion in **1** relative to $Fe^{II}(Br_8TFPP)(Py)_2$, (see below), could account for the decreased Fe–N_p distance. In planar porphyrins, the Fe–N_{ax} bond lengths are longer in Fe^{II} than in Fe^{III} porphyrins[4] and this trend is maintained in **1** [2.028(3) Å] when compared to $[Fe^{III}(OETPP)(Py)_2]ClO_4$ [1.993(3) Å].[32] As a result of the limited structural data available for highly saddled bis-ligated low-spin Fe^{II} and Fe^{III} porphyrins, no meaningful conclusions can be made regarding any relationship between the Fe–N_p or Fe–N_{ax} distances and the oxidation state of the metal.

A normal-coordinate structural decomposition (NSD)[34] analysis of the macrocycle distortions in **1** and several related iron porphyrins are listed in Table 5. The results from the analysis indicate that the predominant distortion in **1** is *sad* with a small *ruf* contribution. Recently, Scheidt et al. reported a correlation between the Fe–N_p distance and the absolute *meso*-carbon displacement in ruffled Fe^{II} and Fe^{III} porphyrins.[35] This correlation does not appear to hold for porphyrins with a saddled conformation within the limited data available.

In saddled porphyrins there is a significant increase in the C_m–C_α–C_β angle and a decrease in the N–C_α–C_β and N–C_α–C_m angles relative to planar porphyrins. This trend holds for **1** and, in addition, there is a ca. 3° increase in the

Table 4. Average bond lengths [Å] and angles [°] for **1** and related complexes.

Complex	Fe–N_p	Fe–N_{Ax}	C_β[c]	C_m[d]	ϕ[e]	Relative orientation[f]
$Fe^{II}(Br_8TFPP)(Py)_2$[33]	1.963(7)	2.012(7)	0.97	0.11	0.7, 21.7	67.8
$Fe^{II}[T(C_3F_7)P](Py)_2$[a][42]	1.958(6)	2.002(6)	0.24	0.62	41.3, 46.0	87.5
1[b]	1.953(3)	2.028(3)	1.22	0.08	11.2, 13.3	87
$[Fe^{III}(OETPP)(Py)_2]ClO_4$[32]	1.957(3)	1.993(3)	1.21	0.05	6.3, 11.6	85.1
Complex	C_α-N–C_α	Fe–N–C_α	N–C_α-C_m	C_m–C_α-C_β	C_α–C_m–C_α	
1[b] *sad*	105.5	125.0	118.9	130.4	126.7	
$Fe^{II}(Br_8TFPP)(Py)_2$[33] *sad*	106.1	125.9	122.5	128.1	123.9	
Fe^{II} $[T(C_3F_7)P](Py)_2$[a][42] *ruf*	105.4	127.3	122.4	128.6	125.5	
$Fe^{II}(TPP)(Py)_2$[4] planar	105.1	127.2	125.9	123.4	123.4	
$[Fe^{III}(OETPP)(Py)_2]ClO_4$[32] *sad*	106.6	123.7	121.8	128.4	121.8	

[a] $T(C_3F_7)P$ is the dianion of *meso*-tetraheptafluoropropylporphyrin. [b] This work. [c] C_β = Average absolute value of the displacement of the pyrrole β carbons from the 24-atom mean plane. [d] C_m = Average absolute value of the displacement of the methine carbons from the 24-atom mean plane. [e] ϕ = Dihedral angle between the plane defined by the closest N_p–Fe–N_{pyr} and the pyridine plane. [f] Relative orientation: dihedral angle between two axial ligands.

Table 5. Out-of-plane displacements (in Å) for the crystal structures of distorted Fe porphyrin complexes from normal-coordinate structural decomposition.[34]

Porphyrin	Total distortion		B_{2u}	B_{1u}	A_{2u}	$E_{g(x)}$	$E_{g(y)}$	A_{1u}
	$d_{obsd.}$	$d_{calcd.}$	d_{sad}	d_{ruf}	d_{dom}	$d_{wav(x)}$	$d_{wav(y)}$	d_{pro}
Fe(OETPP)Cl[43,44]	3.537	3.520	3.478	0.527	0.090	0.020	0.032	0.010
[Fe(OETPP)(Py)$_2$]ClO$_4$[32]	3.682	3.666	3.657	0.147	0.190	0.070	0.031	0.002
Fe(Br$_8$TFPP)Cl[33]	3.322	3.304	3.272	0.408	0.022	0.163	0.112	0.009
Fe(Br$_8$TFPP)(Py)$_2$[33]	3.005	3.000	2.981	0.313	0.046	0.099	0.029	0.017
1[a]	3.752	3.743	3.731	0.237	0.150	0.075	0.067	0.005

[a] This work.

C_α–C_m–C_α angle (Table 4).[4] Another consequence of the increased saddle distortion in **1** is a decrease in the dihedral angle of the *meso*-pyridinum rings relative to the 4N_p plane, 47.3°. However, the average C_m–*meso*–N_{py} distance [1.462(4) Å] does not suggest any significant increased π–π overlap. Similar observations were noted in highly saddled OETPP porphyrins, again without any indication of increased porphyrin–phenyl π overlap.[1,36]

Conclusions

A procedure was developed for the synthesis of iron complexes of [H_2OEPy$_4$P](CF$_3$SO$_3$)$_4$, in three steps starting from Zn(OEP) with an overall yield of ca. 30%. The molecular structure of [Fe(OEPy$_4$P)(Py)$_2$](CF$_3$SO$_3$)$_3$(Br) was determined by X-ray crystallography. The molecule was shown to adopt a severely nonplanar distorted saddle conformation, and the nonplanar macrocycle and its substituents form cavities that orient the axial ligands orthogonally to each other and along the Np–Fe–Np axes. [Fe(OEPy$_4$P)(B)$_2$]$^{4+}$, B = Py or Im, are the first iron complexes of a dodecasubstituted porphyrin bearing four positive charges close to the metal (<5 Å). The Fe^{III}/Fe^{II} redox potentials of +0.62 (B = Py) and +0.38 V (B = Im) (relative to Ag/AgCl) are shifted by as much as ca. +0.7 V when compared to the redox potentials of the corresponding planar complexes of OEP and of the nonplanar, saddle-shaped, complexes of OETPP. These highly positive redox potentials values, that are comparable to those previously reported for dodecasubstituted iron porphyrins bearing electron-withdrawing groups, such as Fe(Br$_8$TFPP)(Py)$_2$ or Fe(F$_{20}$DPP)(Py)$_2$,[33,37] explain the stability of these Fe^{II} porphyrins in air. As previously reported for other iron dodecasubstituted porphyrins bearing electron-withdrawing groups,[29,33,37] the UV/Vis absorption spectra of the [Fe(OEPy$_4$P)(B)$_2$]$^{4+}$ complexes exhibit Soret and visible bands greatly redshifted relative to Fe(OEP)(Py)$_2$. Potential applications in biomedicine, catalysis, and material sciences of these novel iron porphyrins that offer the advantage of being stable in air and also soluble in polar organic solvents as well as in water are currently being pursued.

Experimental Section

Materials and Methods: Methanol (MeOH), diethyl ether (Et_2O) and Celite 545 were purchased from SDS and used without further purification. Trifluoromethanesulfonic acid, Zn(β-octaethylporphyrin = OEP), dichloromethane (CH_2Cl_2), [D_2]dichloromethane (CD_2Cl_2), pyridine (Py), [D_5]pyridine, imidazole (Im), tetraethylammonium hexafluorophosphate (Et_4NPF_6), acetonitrile (MeCN), and Sephadex LH20 were purchased from Aldrich. Tetrabutylammonium perchlorate (Bu_4NClO_4) was obtained from Alfa, pyridine (Py) (extra dry, water <50 ppm) from Acros, and anhydrous $FeBr_2$ and iron powder from Alfa-Ventron.

At BNL, UV/Vis absorption spectra were recorded with a Cary 500 spectrophotometer. Cyclic voltammetry was carried out with a Voltalab 80 electrochemical analyzer. A three-electrode system was used and consisted of a glassy carbon working electrode (GCE, 3.0 mm diameter, BAS), a Pt wire counter electrode, and a Ag/AgCl reference electrode. The solvent was MeCN with 0.1 M Bu_4NClO_4 as the supporting electrolyte and they were purified by standard techniques. ^{1}H NMR spectra were recorded with a Bruker DRX-400 spectrophotometer operating at 400.132 MHz ^{1}H frequency. The NMR spectra were referenced to the residual CD_2Cl_2 solvent peak (δ =5.32 ppm). The DQF-COSY data were recorded at 296 K and processed by using the Xwinnmr software package.

At Paris 5, UV/Vis absorption spectra were recorded with a SAFAS mc2 spectrophotometer operating at room temperature and ^{1}H NMR spectra were recorded at 300 K with a Bruker WR250 spectrometer. Electrochemical experiments were carried out with an EGG-PAR model 173 potentiostat, or with a Tacussel PJT 120–1 potentiostat controlled by a PC computer by a Tacussel IMT-1 interface.

HRMS analyses were carried out at Ecole Polytechnique, Palaiseau, France with a 7-T APEX III FT-ICR mass spectrometer (Bruker Daltonik, Bremen, Germany) equipped with a 7 Tesla actively shielded superconducting magnet and an infinity cell. Nanoelectrospray was used as the ionization source, and nanoelectrospray needles were purchased from Proxeon (Odense, Denmark) and filled with 2 μL of a solution of complex (20 pmol L^{-1} in 50% MeOH/water/0.2% formic acid). Mass spectra were acquired from *m*/*z* 500 to 3000 with 256k data points. MS analysis were performed at "Laboratoire de spectrométrie de masse bio-organique" ECPM, Strasbourg, France with a MicroTof apparatus (Bruker, Wissembourg France) (electrospray).

[Fe(OEPy$_4$P)(Im)$_2$]$^{4+}$: The preparation of Zn(OEPy$_4$P)(PF$_6$)$_4$ from Zn(OEP) was performed as described previously.[21] This complex was demetallated by treatment with CF_3SO_3H.[22] Iron was inserted into the free base porphyrin as follows: H_2OEPy$_4$P(CF$_3$SO$_3$)$_4$ (100 mg, 0.069 mmol) was dissolved in MeOH (3 mL) in the presence of imidazole (5 equiv.). The solution was deoxygenated, anhydrous $FeBr_2$ (36.6 mg, 2.5 equiv.) and Fe powder were added, and the solution was heated at reflux under an argon atmosphere for 18 h. Iron powder was added to reduce the ferric impurities present in $FeBr_2$. After cooling to room temperature, the solution was passed through a short celite column (to remove iron salts). After

evaporation of the solvent, the resulting product was washed with Et_2O (300 mL). Yield: 50 mg (48% assuming a $[Fe(OEPy_4P)(Im)_2]^{4+}$ structure with 4 $CF_3SO_3^-$ counterions as suggested by HRMS). ^1H NMR (250 MHz, CD_3OD, of $[Fe^{II}(OEPy_4P)(Im)_2]^{4+}$ in the presence of 5 equiv. of Im, 300 K): δ = 10.45 (d, J = 6 Hz, 8 H, *o*-H of Py^+), 9.21 (t, J = 7.5 Hz, 4 H, *p*-H of Py^+), 8.65 (dd, J = 6.8 Hz, 8 H, *m*-H of Py^+), 8.18–7.29 (free Im), 5.20 (2 H, bound Im), 3.83 (2 H, bound Im), 3.06 (2 H, bound Im), 2.58 (m, 8 H, CH_2 of CH_2CH_3), 1.15 (m, 8 H, CH_2 of CH_2CH_3), 0.41 (m, 24 H, CH_3) ppm. UV/Vis (CH_3CN containing 100 μM Im, under Ar): λ (ε, $M^{-1}cm^{-1}$) = 366 (70530), 458 (88280), 568 (23250), 601(24170) nm. MS (electrospray, TOF): m/z = 1347.4 $[Fe(OEPy_4P)(CF_3SO_3)_3]^+$, 1279.3 $[Fe(OEPy_4P)(CF_3SO_3)_2(Br)]^+$, 599.3 $[Fe(OEPy_4P)(CF_3SO_3)_2]^{2+}$, 349.9 $[Fe(OEPy_4P)(CF_3SO_3)]^{3+}$, 326.8 $[Fe(OEPy_4P)(Br)]^{3+}$, 225.7 $[Fe(OEPy_4P)]^{4+}$.

$[Fe(OEPy_4P)(Py)_2]^{4+}$: A dichloromethane solution of the above $[Fe^{II}(OEPy_4P)(Im)_2]^{4+}$ complex was treated with an excess of pyridine (5% vol). The NMR sample was prepared directly in the NMR tube by adding an excess of [D_5]pyridine to a CD_2Cl_2 solution of the $[Fe^{II}(OEPy_4P)(Im)_2]^{4+}$ complex. ^1H NMR [400 MHz, CD_2Cl_2 containing 5% (vol) of C_5D_5N, 296 K]: δ = 10.46 (d, J = 6 Hz, 8 H, *o*-H of Py^+), 8.99 (t, J = 7.5 Hz, 4 H, *p*-H of Py^+), 8.45 (t, J = 6.8 Hz, *m*-H of Py^+), 2.48 (m, 16 H, CH_2 of CH_2CH_3), 0.22 (t, J = 7.1 Hz, 24 H, CH_3). The peaks assignments were made from the DQF-COSY spectrum. UV/Vis (CH_3CN): λ = 366, 439, 458, 556, 588 nm.

Crystallography: Selected crystallographic experimental data are presented in Table 6. Crystals of $[Fe(OEPy_4P)(Py)_2](CF_3SO_3)_3(Br)$ were grown by vapor diffusion of pentane into a solution of the complex in CH_2Cl_2. A crystalline sample was placed in Paratone-N, the single crystal was suspended in a nylon loop and transferred to the liquid nitrogen cold stream of the diffractometer. Crystallographic data were collected at beamline X26C of the National Synchrotron Light Source at Brookhaven National Laboratory. 360° of data were collected by the rotation method on an ADSC Quantum 4 area detector and processed with Denzo/Scalepack. Lattice parameters for the synchrotron data were determined separately for each recorded image and are mean values derived from the reproducibility of the determinations. The structures were solved by direct methods and refined against F^2 by using SHELXL-97 in the SHELXTL version 5 package. Hydrogens were included in idealized positions by using a riding model. CCDC-630557 contains the supplementary crystallographic data for this paper. These data can be obtained free of charge from The Cambridge Crystallographic Data Centre via www.ccdc.cam.ac.uk/data_request/cif.

Table 6. Crystallographic details for $[Fe(OEPy_4P)(Py)_2](CF_3SO_3)_3(Br)$ (**1**).

Empirical formula	$C_{69}H_{70}BrF_9FeN_{10}O_9S_3$
Formula mass [g mol^{-1}]	1586.28
Space group	$P2_1/c$
T [K]	103(2)
a [Å]	14.261(3)
b [Å]	26.501(5)
c [Å]	21.202(4)
α [°]	90.00
β [°]	107.52(3)
γ [°]	90.00
V [Å^3]	7641(3)
Z	4
λ [Å]	0.8950
$D_{calcd.}$ [g cm^{-3}]	1.435
μ [mm^{-1}]	0.890
R_1 [$F_o > 4\sigma(F_o)$]	0.0686
wR_2 (all data)	0.2021

Supporting Information (see footnote on the first page of this article): ^1H NMR spectrum of the $[Fe(OEPy_4P)(Im)_2]^{4+}$ complex and a figure illustrating the hydrogen bond between the pyridine C59···H and a triflate anion oxygen atom.

Acknowledgments

The work at Brookhaven was supported by the Offices of Biological and Environmental Research and of Basic Energy Sciences of the US Department of Energy under Contract No. DE-AC02-98CH10886, and by the National Center for Research Resources of the National Institutes of Health. Financial support for C. B., D. M., and P. B. came from CNRS and University Paris 5. The authors thank Drs. A. Giraudeau, A. Brisach-Wittmayer (UMR 7512, Strasbourg, France) and L. Ruhlmann (Université Paris-Sud, Orsay, France) for their crucial help in the synthesis of Zn(OEPy$_4$P)(PF$_6$)$_4$ and for a gift of this complex at the beginning of this work. We also thank Dr. J. Fajer for important discussions and help during this work, and Dr. Chamot-Rooke (Laboratoire des Mécanismes Réactionnels, Palaiseau, France) for HRMS measurements.

[1] M. O. Senge, "Highly Substituted Porphyrins" in *The Porphyrin Handbook* (Eds.: K. M. Kadish K. M. Smith, R. Guilard), Academic Press, New York, **2000**, vol. 1, ch. 6, p. 239.
[2] M. O. Senge, *Chem. Commun.* **2006**, 243–256.
[3] F. A. Walker, *Chem. Rev.* **2004**, *104*, 589–615.
[4] W. R. Scheidt, "Systematics of the Stereochemistry of Porphyrins and Metalloporphyrins" in *The Porphyrin Handbook* (Eds.: K. M. Kadish, K. M. Smith, R. Guilard), Academic Press, New York, **2000**, vol. 3, ch. 16, p. 49.
[5] M. W. Renner, K. M. Barkigia, J. Fajer, *Inorg. Chim. Acta* **1997**, *263*, 181–187.
[6] K. M. Kadish, E. Van Caemelbecke, G. Royal, "Electrochemistry of Metalloporphyrins in Nonaqueous Media" in *The Porphyrin Handbook* (Eds.: K. M. Kadish, K. M. Smith, R. Guilard), Academic Press, New York, **2000**, vol. 8, ch. 55, p. 1.
[7] B. Meunier, A. Robert, G. Pratviel, J. Bernardou, "Metalloporphyrins in Catalytic Oxidations and Oxidative DNA Cleavage" in *The Porphyrin Handbook* (Eds.: K. M. Kadish, K. M. Smith, R. Guilard), Academic Press, New York, **2000**, vol.4, ch. 31, p. 119.
[8] D. Dolphin, T. G. Traylor, L. Y. Xie, *Acc. Chem. Res.* **1997**, *30*, 251–259.
[9] D. Mansuy, *Coord. Chem. Rev.* **1993**, *125*, 129–142.
[10] E. D. Sternberg, D. Dolphin, C. Brückner, *Tetrahedron* **1998**, *54*, 4151–4202.
[11] Z. Ziegler, L. Pasierb, K. A. Cole, D. W. Wright, *J. Inorg. Biochem.* **2003**, *96*, 478–486.
[12] J. P. C. Tomé, M. G. P. M. S. Neves, A. C. Tomé, J. A. S. Cavaleiro, M. Soncin, M. Magaraggia, S. Ferro, G. Jori, *J. Med. Chem.* **2004**, *47*, 6649–6652.
[13] A. V. Vzorov, D. W. Dixon, J. S. Trommel, L. G. Marzilli, R. W. Compans, *Antimicrob. Agents Chemother.* **2002**, 3917–3925.
[14] R. W.-Y. Sun, W.-Y. Yu, H. Sun, C.-M. Che, *ChemBioChem* **2004**, *5*, 1293–1298.
[15] W. S. Caughey, L. D. Raymond, M. Horiuchi, B. Caughey, *Proc. Natl. Acad. Sci. USA* **1998**, *95*, 12117–12122.
[16] I. Batinic-Haberle, I. Spasojevic, P. Hambright, L. Benov, A. L. Crumbliss, I. Fridovich, *Inorg. Chem.* **1999**, *38*, 4011–4022.
[17] T. P. Misko, M. K. Highkin, A. M. Veenhuinzen, P. T. Manning, M. K. Stern, M. G. Currie, D. Salvemini, *J. Biol. Chem.* **1998**, *273*, 15646–15653.
[18] J. Lee, J. A. Hunt, J. T. Groves, *J. Am. Chem. Soc.* **1998**, *120*, 6053–6061.

[19] I. Batinic-Haberle, S. I. Liochev, I. Spasojevic, I. Fridovich, *Arch. Biochem. Biophys.* **1997**, *343*, 225–233.
[20] R. Weiss, F. Pühlhofer, N. Jux, K. Merz, *Angew. Chem. Int. Ed.* **2002**, *41*, 3815–3817.
[21] A. Giraudeau, S. Lobstein, L. Ruhlmann, D. Melamed, K. M. Barkigia, J. Fajer, *J. Porphyrins Phthalocyanines* **2001**, *5*, 793–797.
[22] C. Bochot, J.-F. Bartoli, Y. Frapart, P. M. Dansette, D. Mansuy, P. Battioni, *J. Mol. Catal., A* **2007**, *263*, 200–205.
[23] L. Ruhlmann, S. Lobstein, M. Gross, A. Giraudeau, *J. Org. Chem.* **1999**, *64*, 1352–1355.
[24] K. Ozette, P. Battioni, P. Leduc, J.-F. Bartoli, D. Mansuy, *Inorg. Chim. Acta* **1998**, *272*, 4–6.
[25] J.-F. Bartoli, V. Mouries-Mansuy, K. Le Barch-Ozette, M. Palacio, P. Battioni, D. Mansuy, *Chem. Commun.* **2000**, 827–828.
[26] K. M. Barkigia, L. Chantranupong, K. M. Smith, J. Fajer, *J. Am. Chem. Soc.* **1988**, *110*, 7566–7567.
[27] M. O. Senge, R. W. Renner, W. W. Kalisch, J. Fajer, *J. Chem. Soc., Dalton Trans.* **2000**, 381–385.
[28] P. Ochsenbein, K. Ayougou, D. Mandon, J. Fischer, R. Weiss, R. N. Austin, K. Jayaraj, A. Gold, J. Terner, J. Fajer, *Angew. Chem. Int. Ed. Engl.* **1994**, *33*, 348–350.
[29] J.-F. Bartoli, K. Le Barch, M. Palacio, P. Battioni, D. Mansuy, *Chem. Commun.* **2001**, 1718–1719.
[30] K. M. Barkigia, M. Palacio, Y. Sun, M. Nogues, M. W. Renner, F. Varret, P. Battioni, D. Mansuy, J. Fajer, *Inorg. Chem.* **2002**, *41*, 5647–5649.
[31] K. Ozette, P. Leduc, M. Palacio, J.-F. Bartoli, K. M. Barkigia, J. Fajer, P. Battioni, D. Mansuy, *J. Am. Chem. Soc.* **1997**, *119*, 6442–6443.
[32] M. Nakamura, *Coord. Chem. Rev.* **2006**, *250*, 2271–2294.
[33] M. W. Grinstaff, M. G. Hill, E. R. Birnbaum, W. P. Schaefer, J. A. Labinger, H. Gray, *Inorg. Chem.* **1995**, *34*, 4896–4902.
[34] L. Sun, W. Jentzen, J. A. Shelnutt, *The Coordinate Structural Decomposition Engine*, http://jasheln.unm.edu.
[35] C. Hu, B. C. Noll, C. E. Schulz, W. R. Scheidt, *Inorg. Chem.* **2005**, *44*, 4346–4358.
[36] K. M. Barkigia, M. D. Berber, J. Fajer, C. J. Medforth, M. W. Renner, K. M. Smith, *J. Am. Chem. Soc.* **1990**, *112*, 8851–8857.
[37] K. M. Kadish, E. Van Caemelbecke, F. D'Souza, M. Lin, D. J. Nurco, C. J. Medforth, T. P. Forsyth, B. Krattinger, K. M. Smith, S. Fukuzumi, I. Nakanishi, J. A. Shelnutt, *Inorg. Chem.* **1999**, *38*, 2188–2198.
[38] V. P. Shedbalkar, L. B. Dugad, S. Mazumdar, S. Mitra, *Inorg. Chim. Acta* **1988**, *148*, 17–20.
[39] L. Edwards, D. H. Dolphin, M. Gouterman, *J. Mol. Spectrosc.* **1970**, *35*, 90–109.
[40] R. Bonnett, M. J. Dimsdale, *J. Chem. Soc., Perkin Trans. 1* **1972**, 2540–2548.
[41] K. M. Kadish, E. Van Caemelbecke, G. Royal, "Electrochemistry of Metalloporphyrins in Nonaqueous Media: Data Bases of Redox Potentials Media" in *The Porphyrin Handbook* (Eds.: K. M. Kadish, K. M. Smith, R. Guilard), Academic Press, New York, **2000**, vol. 9, ch. 59, p. 1.
[42] K. T. Moore, J. T. Fletcher, M. J. Therien, *J. Am. Chem. Soc.* **1999**, *121*, 5196–5209.
[43] R.-J. Cheng, P.-Y. Chen, P.-R. Gau, C.-C. Chen, S.-M. Peng, *J. Am. Chem. Soc.* **1997**, *119*, 2563–2569.
[44] V. Schünemann, M. Gerdan, A. X. Trautwein, N. Haoudi, D. Mandon, J. Fischer, R. Weiss, A. Tabard, R. Guilard, *Angew. Chem. Int. Ed.* **1999**, *38*, 3181–3183.

Received: December 12, 2006
Published Online: May 4, 2007

